RSC Advances

ROYAL SOCIETY OF CHEMISTRY

www.rsc.org/advances

Multijet motion and deviation in electrospinning

Yuansheng Zheng,[a] R. Hugh Gong[b] and Yongchun Zeng[a, c,*]

a. Textile Engneering, College of Textiles, Donghua University, Shanghai, 201620, People's Republic of China. Email: yongchun@dhu.edu.cn.

b. Textiles & Paper, School of Materials, The University of Manchester, Manchester, M13 9PL, UK.

c. Key Laboratory of Textile Science & Technology, Donghua University, Ministry of Education, Shanghai, 201620, People's Republic of China.

This study provides a thorough description associated with multijet motion and deviation in electrospinning.

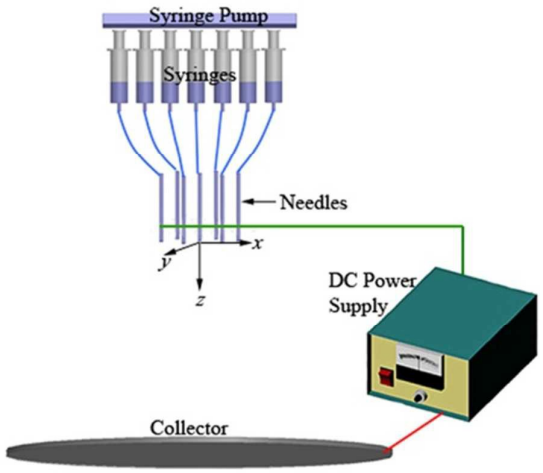

RSC Advances

ARTICLE

Multijet motion and deviation in electrospinning

Yuansheng Zheng,[a] R. Hugh Gong[b] and Yongchun Zeng[a, c,]*

Received 00th January 20xx,
Accepted 00th January 20xx

DOI: 10.1039/x0xx00000x

www.rsc.org/

Electric field plays a key role in the electrospinning process. The electrospinning process is governed by the electric filed caused by the applied voltage between the spinneret and the collector. In the present work, a comprehensive analysis was carried out to investigate the effect of the electric field on jet behavior in the multijet electrospinning process. Two multijet electrospinning systems were involved in this study. High-speed photography was adopted to capture the jet motion, and numerical simulation was used to understand the electric field distribution. The characteristics of jet behavior were described with five parameters: the straight jet length of central jet, the straight jet length of outer jet, the envelope cone of the central jet, the envelope cone of outer jet, and the deviation angle of the outer jet. It was observed that all the parameters are influenced by the applied voltage and induced electric field distribution. It was found that the shape and strength of the electric field are the two factors responsible for the jet behavior in the multijet electrospinning system.

Introduction

Electrospinning process has been widely explored as a method to fabricate nanofibrous nonwowens. However, the low fiber production rate (usually 0.01~0.1 g/h from single jet) has limited the industrial application of this technology. Various approaches have been reported to scale up nanofiber production in the last few years. These approaches can be summarized as: multijet electrrospinning such as multineedle electrospinning,[1,2] and multihole electrospinning,[3-5] and free surface electrospinning.[6-8]

The most difficult issue in the multijet electrospinning process is the deviation of the jets, which always causes instability problems such as dripping of the polymer solution and fiber collection difficulties. To control the multijet electrospinning process, a variety of configurations, such as extra electrode,[1, 9] and auxiliary plate,[10, 11] have been introduced into multijet electrospinning to modify the electric field. Deitzel et al. demonstrated a control system using three power supplies and eight rings, which could dampen the electrospinning instability.[12] Kim designed an electrospinning process with a cylindrical auxiliary electrode connected to a spinning nozzle to stabilize the initial spun solution and control the spun jets.[9] Yang et al. used a shield ring to modify the electric field distribution and control the jet path in a multineedle electrospinning process.[1] Xie and Zeng adopted an auxiliary plate electrode to obtain more uniform electric field in a multineedle system.[11] Although considerable work has been done to understand and control the multijet spinning process, detailed understanding of the jet deviation in multijet electrospinning is still unavailable. The jet-jet interaction was first described by Theron et al. experimentally and numerically.[2] Kumar et al. discussed the jet repulsion in multijet electrospinning.[13] With the above mentioned information, it is known that jet deviation in the multijet electrospinning process is attributed to two main factors: (a) the surface charges carried by the jets causing jet repulsion, and (b) the diverging shape of the electric field lines leading to jet offset. The important role of electric field in electrospinning has been widely recognized. The impact of electric fields at the molecular level on the polymer chains has been reported.[14, 15] This study focuses on the effect of electric fields on the jet motion.

Our previous studies show that the electric field distribution plays a significant role in jet behavior, the resultant fibers and fiber mats in the single-jet and the multjet electrospinning processs.[16, 17] The aim of the present work is to explore the effect of the electric field distribution on the jet motion and the jet deviation in multijet electrospinning. A multihole electrospinning configuration and a multineedle electrospinning configuration with different electric fields were involved in the study. Numerical simulation is used to understand the three-dimensional (3D) electric fields. The experiments are carried out with the two mutlijet electrsopinning systems to compare the jet behavior in different electric fields. Five parameters are measured to characterize the jet behavior in the spinning process. The jet deviation in multijet electrospinning is studied based on the experimental and simulation results.

Experiments and simulation

Material preparation

[a] Textile Engneering, College of Textiles, Donghua University, Shanghai, 201620, People's Republic of China. Email: yongchun@dhu.edu.cn.
[b] Textiles & Paper, School of Materials, The University of Manchester, Manchester, M13 9PL, UK.
[c] Key Laboratory of Textile Science & Technology, Donghua University, Ministry of Education, Shanghai, 201620, People's Republic of China.

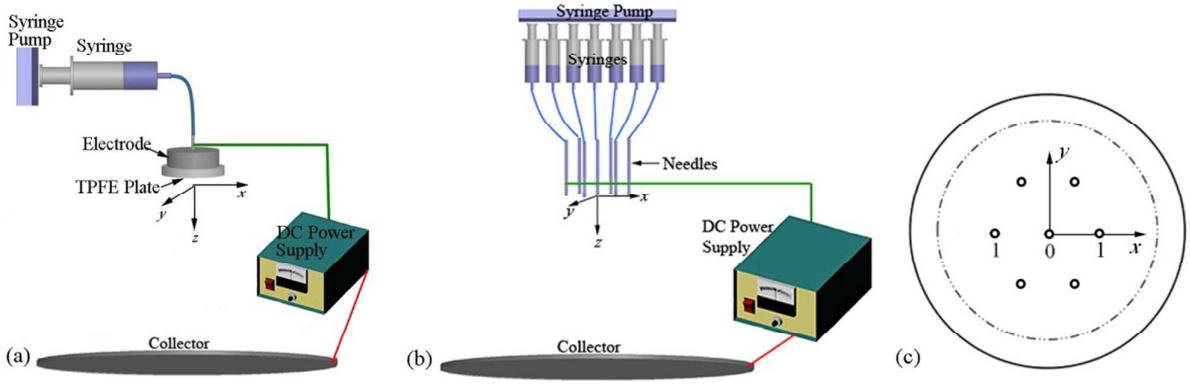

Fig. 1 Schematics of experimental setups: (a) flat spinneret electrospinning, (b) multineedle electrospinning and (c) hole / needle distribution.

Table 1 The experiment processing parameters for the two electrospinning configurations

Group	Applied voltage (kV)	Needle/hole distance (mm)	Working distance (cm)	Flow rate (ml/h)
Multihole	25, 30, 35	10	25	3.5
Multineedle	15, 20, 25	15		

Polyethylene oxide (PEO, *Mw* = 600 000 g/mol, Sigma-Aldrich, Inc., USA) was used as received. PEO powder was dissolved in distilled water with 6.0 wt% concentration, and the solution was prepared at ambient temperature. The solution viscosity was 970 mPa.s, and the solution conductivity was 95.28 μs/cm. All the experiments were done in the controlled conditions: temperature 25 ± 3°C, humidity 60 ± 5%.

Experimental Setup

In this study, two multijet electrospinning systems, a multihole flat spinneret electrospinning setup (Figure 1a) and a conventional multineedle electrospinning setup (Figure 1b), were investigated. As detailed elsewhere, the spinneret of the multihole setup, which was called the flat spinneret, was composed of a flat electrode and a plastic plate. The plastic plate with holes drilled on it was used for the creation of jets.[17] In this study, a seven-hole flat spinneret was used. The holes with 0.5-mm diameter on the plate surface were equilateral hexagon distributed as shown in Figure 1c. The electrode was made of aluminum with 50-mm diameter and 20-mm height. A solution chamber was formed between the flat electrode and the plastic plate. A 2-mm-outer-diameter metallic tube was inserted in the center of the aluminum electrode, and an insulated tube with 2-mm outer diameter linked the syringe to the metallic tube which provided solution feeding.[17] In the multineedle setup, the spinneret was made of seven blunt-tip type metal needles with 0.8-mm outer diameter, 0.5-mm inner diameter and 36-mm length. The needles were also hexagon distributed.

The polymer solution was forced from a syringe via a syringe pump (KDS 220, KD Scientific, Inc. USA) to the spinneret. The solution flow rate was set to 0.5 ml/h. A high voltage power supply (ES-60P 10W/DDPM, Gamma High Voltage Research, USA) was applied to the spinneret and the aluminum foil-grounded collector. The distance between the spinneret and the collector was set to 25 cm. The processing parameters for the multihole and multineedle electrospinning experiments are shown in Table 1. All the electrospinning experiments were carried out at room temperature and normal atmospheric pressure.

Electric Field Simulation

The 3D electric fields were simulated by Ansoft Maxwell (ANSYS Inc., USA) software using the finite element method (FEM). Before the simulation, the physical geometries of the electrospinning setups (e.g., spinneret and collector), polymer solution in the chamber and needles were established according to their practical dimensions, locations, and relative permittivities. The aluminum collector and the boundaries at an infinite distance were set as zero potential. The meshing and solving were performed by the software to obtain the electric field intensity and profile.

The electric field lines of the two electrospinning configurations were analyzed by COMSOL Multiphysics® Finite Elemental Analysis software.

Jet Path Record

The jet motions in the multijet electrospinning processes were captured by a Redlake HG-100K high-speed camera (Redlake Inc., San Diego, USA) with long exposure times. Image processing and analysis were done with ImageJ image analysis software (NIH, USA).

Simulation results

To explore the effect of the electric field on the jet motion, the 3D models of the seven-hole and the seven-needle electrospinning systems were created to simulate the electric filed distributions and the electric field lines. Figure 2 shows the electric field distributions of the multihole and the multineedle electrospinning configurations simulated by Ansoft Maxwell 3D software. The simulation results show that the multihole spinneret creates a relatively uniform electric field on the surface of the spinneret (Figure 2a), while an extremely high electric field concentrates in the surrounding area of the needles for the multineedle configuration (Figure 2b). These observations can be further confirmed by Figures 2c and 2d. Compared with the multineedle configuration, the multihole configuration creates a much larger area of uniform electric field in the same horizontal plane.

Figure 3 shows the calculated electric field intensity of the two electrospinning configurations. The electric field intensity along the

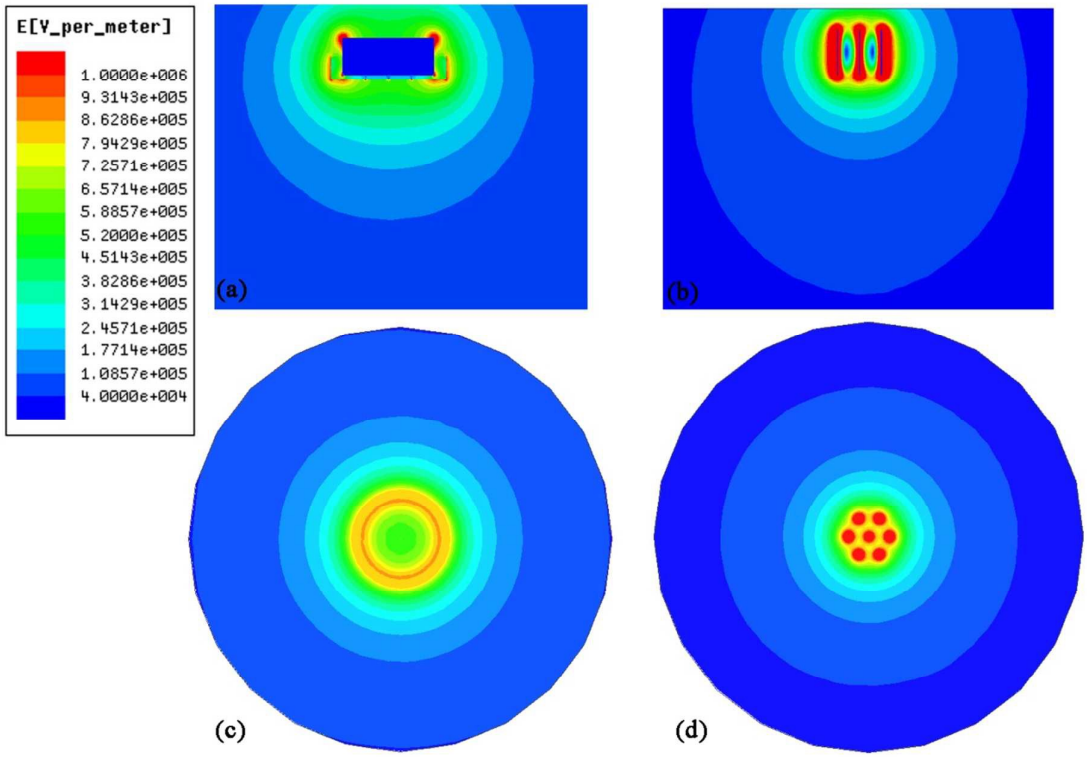

Fig. 2 Comparison of the electric field distributions for the two electrospinning configurations with a working distance of 25 cm and an applied voltage of 25 kV: (a) center plane along *z*-axis of multihole configuration, (b) center plane along *z*-axis of multineedle configuration, (c) horizontal plane along *xy*-plane at *z* = 1 mm of multihole configuration and (d) horizontal plane along *xy*-plane at *z* = 1 mm of multneedle configuration.

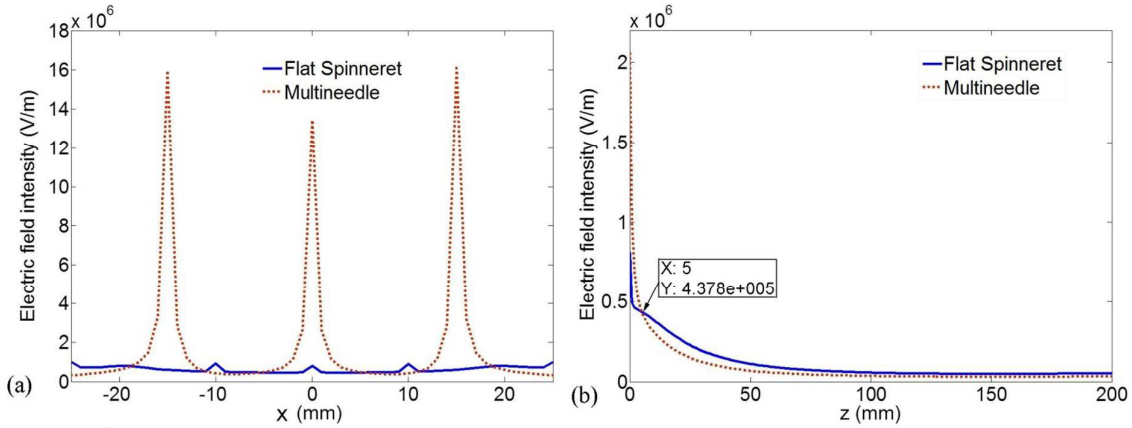

Fig. 3 The electric field intensity for the two configurations with a working distance of 25 cm and an applied voltage of 25 kV: (a) *E* distribution along *z*-axis at central line, and (b) *E* distribution along *y*-axis.

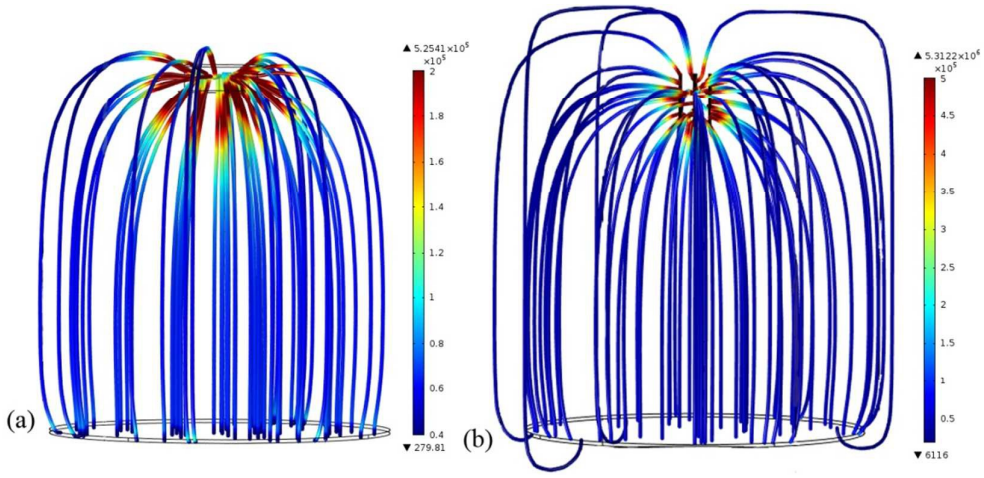

Fig. 4 Electric field lines simulated by Comsol Multiphysics software: (a) the flat spinneret configuration, and (b) the multineedle configuration.

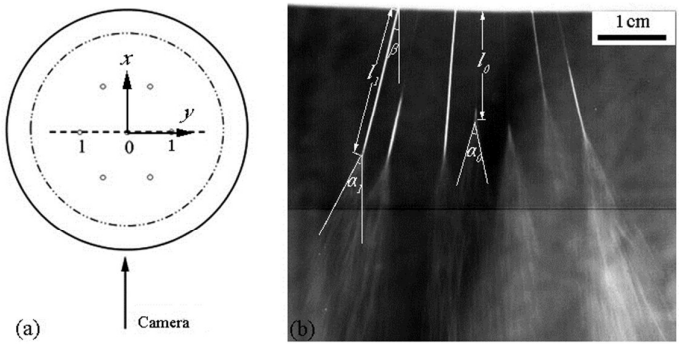

Fig. 5 The illustration of the captured jet motion in a multijet electrospinning process: (a) arrangement of the holes/needles, and (b) the characteristic parameters for the multijet electrospinning.

x-axis on the spinneret surface shown in Figure 3a indicates that for the multineedle system, the electric field intensifies at the needle tip. The maximum electric field intensity E at the side needle tip is 1.61×10^7 V/m in the case of the multineedle configuration and 9.15×10^5 V/m in the case of the multihole configuration at 25 kV applied voltage. It is also shown that the electric field intensity at the side needle positions is higher than that at the central needle. While for the multihole system, the difference of electric field intensity at the side-hole positions and the central-hole position is much smaller. Figure 3b shows the electric field intensities along the *z*-axis (i.e. spinning direction) at the central line for the two multijet electrospinning configurations. There is a sharp decrease of electric field intensity below the spinneret at the central line for the multineedle system. It is obvious that the multihole system creates a more uniform electric field distribution. More importantly, the flat spinneret system creates higher electric field intensity except in the area very close to the spinneret (z < 5 mm).

The simulated electric lines for the two types of spinneret simulated by the COMSOL Multiphysics software are shown in Figure 4. Compared with the multihole system, the electric field lines generated in the multineedle configuration are more scattered outward at the needle area.

Results and discussion

Jet Motion and Characteristic Parameter

Figure 5a illustrates the jet motion captured in the seven-jet electrospinning process. The filming direction is along the *x*-axis. It is seen that the behavior of the central jet develops in the same way as the jet in a single-jet process, while those on the sides are pushed outward away from the center. The jet at position 0 in Figure 5a is referred to as the central jet, and the jet at position 1 is referred to as the outer jet in this study. To characterize the jet motion in multijet electrospinning, five parameters are defined and shown in Figure 5b: (1) the straight jet length of the central jet, l_0; (2) the envelope cone of the central jet, α_0; (3) the straight jet length of the outer jet, l_1; (4) the envelope cone of the outer jet, α_1; and (5) the deviation angle of the outer jet, β. It is well-known that the electrospun jet typically has an almost straight section followed by a whipping section. The straight jet length is defined as the straight section of the jet path. The envelope cone is used to determine the extent of whipping, or the whipping amplitude. The deviation angle determines the offset of the outer jets from the central line.

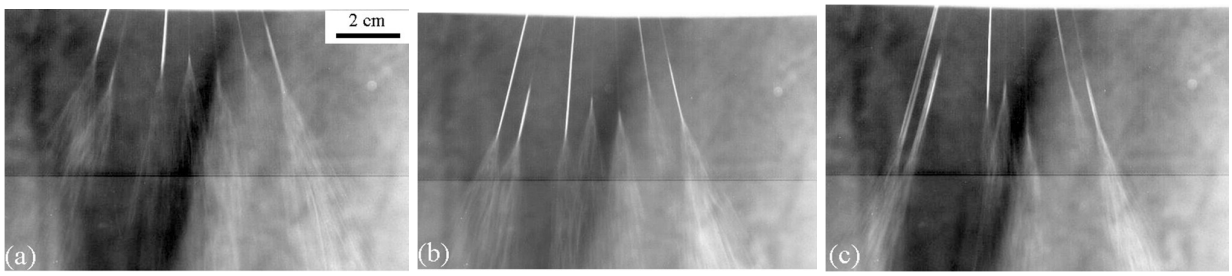

Fig. 6 The jet behavious in the multihole electrospinning process with various applied voltages: (a) 25 kV; (b) 30 kV; and (c) 35 kV.

Jet Behavior in Multihole Electrospinning

Jet Motion: In this section, the jet motion in the multihole electrospinning process is investigated to explore the behavior of jet deviation. Figure 6 shows the jet motion of the seven-hole electrospinning process with various applied voltages. It can be observed that the straight jet lengths of the central jet and the outer jets, l_0 and l_1, increase with increasing applied voltage. The deviation angle of the outer jet, β, decreases with increasing applied voltage, indicating that the jets are more concentrated with a higher applied voltage. The measurement results of the five parameters shown in Table 2 further illustrate these observations. It is seen from Table 2 that under the same applied voltage, the straight jet length of the outer jet is longer than that of the central jet, and the envelope cone of the outer jet is larger than that of the central jet, implying that the central jet motion is depressed by the outer jets. With an increase in applied voltage, the straight jet length increases for both the central jet and the outer jet, and the deviation angle of the outer jet increases. On the contrary, the envelope cones for both the outer jet and the central jet decrease in size with the increase of applied voltage.

Straight jet length: Figure 7 shows the calculated electric field strengths for the multihole electrospinning configurate under different applied voltages. It can be observed that the distributions of the electric field intensity along the *y*-axis at various voltages have the same tendency, and the electric filed intensity inceases with voltage. Also shown is that the electric field intensity at the central hole is smaller than that at the side holes, indicating that the electric field strength at the central hole is weakened by the side holes surrounding it. Angammana and Jayaram drew the same conclusion in their study on the multineedle electrospinning process.[18]

The interaction of applied electric field with the electrostatic

Table 2 The measurement results of l_0, α_0, l_1, α_1, β in the multihole electrospinning process

Applied Voltage (kV)	l_0 (cm)	α_0 (deg)	l_1 (cm)	α_1 (deg)	β (deg)
25	3.31	25.67	4.26	28.94	15.23
30	4.73	20.89	5.33	27.61	13.49
35	4.65	14.01	6.03	20.66	13.23

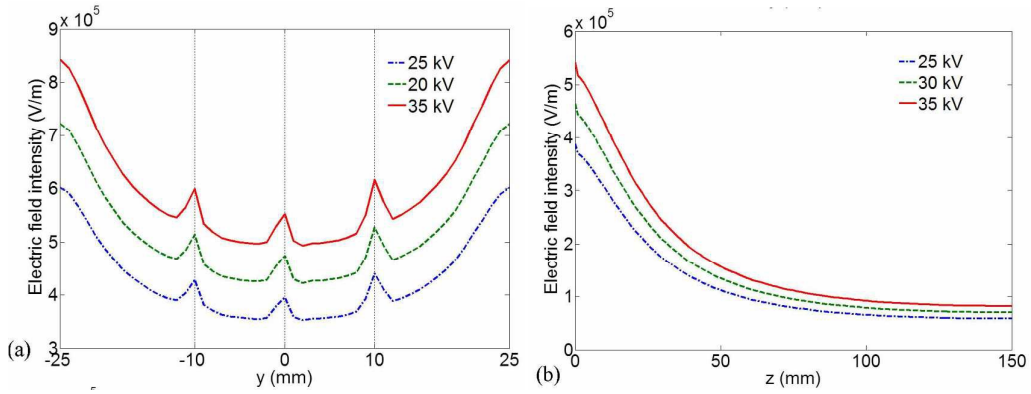

Fig. 7 The electric field intensities of the multihole electrospinning configuration: (a) along *y*-axis at z = 1 mm; and (b) along *z*-axis at central line.

charges at the fluid surface results in the ejection of straight fluid jet.

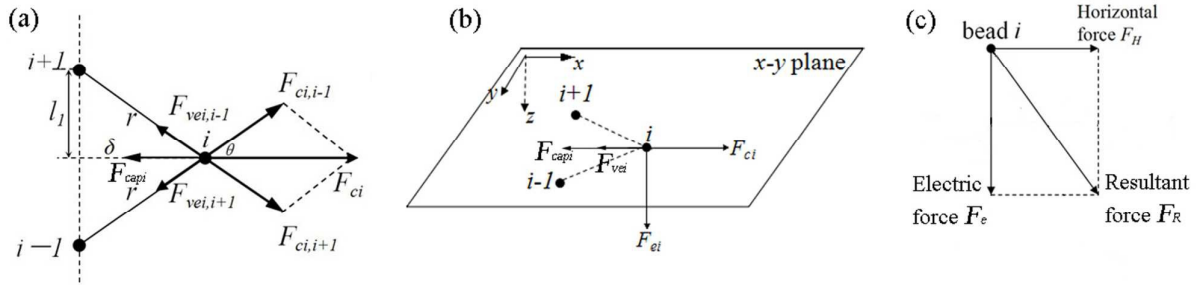

Fig. 8 Illustrations of jet whipping in the electrospinning process.

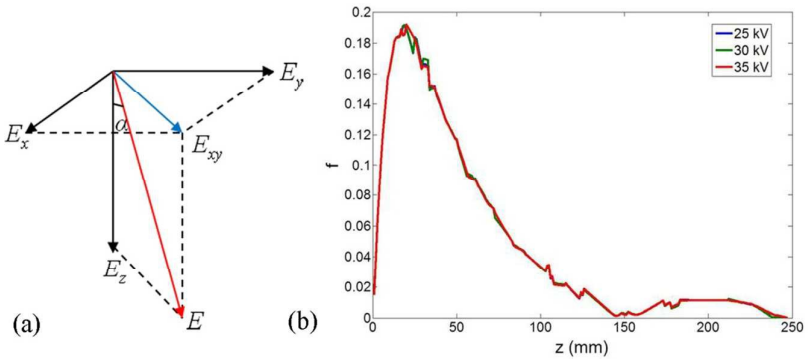

Fig. 9 (a) Illustration of *α* and (b)calculated *f* for various applied voltages.

Some researchers have observed that a higher electric field leads to a greater streching of the jet.[19, 20] Based on this observation, the higher electric field strength at side holes leads to a longer straight jet length in our experiments. Figure 7b shows the variation of the electric field intensity along the *z*-axis with the voltages. It is obvious that the electric field decays along the spinning direction, with a sharper weakening in the area near the spinneret. Both Figures 7a and 7b show that a higher applied voltage produces a higher electric field intensity, especially in the area near the spinneret, and therefore results in longer straight jet lengths of the central and outer jets.

Envelope cone: The reason for the observed phenomenum that a higher applied voltage provides a higher electric force rusulting in a smaller envolpe cone may be understood in the following way. The mechanism of the electrically driven bending instability of jets in electrospinning has been analyzed by Reneker and co-workers.[21] They chose a jet element (*i*-1, *i*+1) and treated it as three point-like charges, each with a value *e*, shown in Figure 8a. If a small perturbation causes point *i* to move off the line, a net Coulomb force $\mathbf{F}_{ci}$ acts on *i* in a direction perpendicular to the rectilinear jet, and causes *i* to move further away from the line in the direction of the perturbation. The Coulomb force $\mathbf{F}_{ci}$ sustains the increase of the perturbation, while the viscoelastic force F_{vei} and the surface tension force $\mathbf{F}_{capi}$ tend to counteract the bending perturbation. If the Coulomb force is larger than the viscoelastic force and the surface tension force, the bending perturbation continues to grow and develops into whipping instability.

The forces acting on bead *i* (the imaginary bead is not the same as the physical bead) of the electrospun jet element are shown in Figure 8b. In the *x*-*y* plane, the Coulomb force and the surface tension force depend on the relative position of beads *i*-1 and *i*, whereas the viscoelastic force depends on the relative speed of beads *i*-1 and *i*. The normal force perpendicular to the *x*-*y* plane (i.e. *z* direction), the electric force $\mathbf{F}_{ei}$, is determined by the the electric field strength. The horizontal force $\mathbf{F}_{H}$ indicates the resultant force in the *x*-*y* plane, which is shown in Figure 8c. As a result, the horizontal force is not influenced by the electric field strength. As shown in Figure 8c, when the electric field force increases, the angle of the final resultant force $\mathbf{F}_{R}$ along the *z*-axis decreases, implying the decrease of the envelop cone of whipping. It has been shown that the electric field strength increases with increasing applied voltage (see Figure 7), indicating that higher applied voltages lead to smaller envolpe cones.

Deviation angle of the jet: For a given configuration of the electrospinning setup, including the spinneret, the collector and their positions, the electric field lines are determined. The shape of the electric field is not influenced by the applied voltage. To explain this, a parameter *f* is defined to describe the deviation of the electric field lines [15]. It is calculated as

$$f = \frac{\sqrt{E_x^2 + E_y^2}}{|E_z|} \qquad (1)$$

where E_x, E_y and E_z are the components of the electric field strength *E* along *x*, *y* and *z* axis, respectively, as shown in Figure 9a. *f* is the tangent of the included angle *α* of the spinning direction and *E*. Figure 9b shows the comparison of *f* along the spinning direction for the various applied voltages. As illustrated, the *f* value is exactly the same under three different voltages.

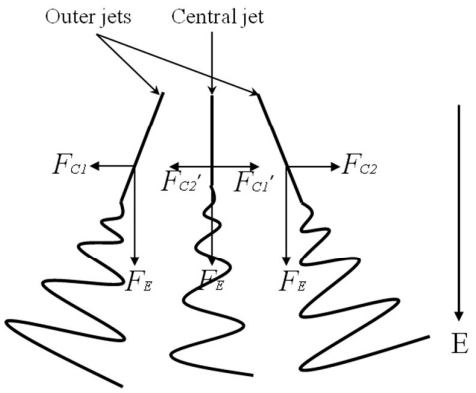

Fig. 10 Force analysis of the straight jet part in the electrospining process.

For the given seven-hole configuration, the shape of the electric field lines is determined. For the two factors that cause jet deviation discussed by previous work,[11, 22] the surface charges on the jet and the shape of the electric field created from the spinneret to the collector, the latter does not need to be considered here. As to the the surface charges on the jet, our previous study illustrated that higer electric field intensities produce more surface charges on the jets and consequently larger repulsion forces according to the Coulomb's law.[22] This is contrary to the experimental result shown in Figure 6 and Table 2 which indicate that the deviation angle of the outer jet (β) decreases with increasing applied voltage (and therefore the electric field strength). It appears that there is another factor influencing jet deviation in multijet electrospinning.

To explore this factor, the forces acting on the central and outer jets during multijet electrospinning is analyzed in Figure 10. The path of the central jet develops in the same way as that in the single-jet electrospinning due to the symmetrical arrangement of the side jets, while the paths of the outer jets are deviated by Coulomb force. Besides the electric field force $\mathbf{F}_E$, the Coublomb force $\mathbf{F}_C$ are exerted on each jet by their neighbors. As illustrated, the electric field force increases with the incease of the electric field strength, which may lead to smaller deviation angle of the outer jet. Thus it can be seen that jet diviation is also affectd by the electric field force for a given electrospinning configuration.

Multineedle electrospinning

Figure 11 shows the jet behaviors in the seven-needle electrospinning configuration with various applied voltages, and the measured results of the characteristic parameters are presented in Table 3. The results confirm the same observation as in the multihole electrospinning process under the same applied voltage. The straight jet length of the outer jet is longer than that of the central jet, and the envelop cone of the outer jet is larger than that of the central jet. It is observed that with increasing applied voltage, all the five parameters, the straight lengths and the envelop cones of the central jet and the outer jet, and the deviation angle of the outer jet, increase. It is worth mentioning that when the applied voltage is 15 kV, the electric force is not strong enough and the jet cannot eject from the central needle. However, unlike the case for the multihole configuration, the outer jet deviation angle and the envelope cone increase with increasing applied voltage.

Compared with the multihole configuration, the multineedle configuration creates much larger envelop cones and outer jet deviation angles. Moreover, the difference between the envelop cones of the central jet and the outer jet is much larger, implying that the shielding effect on the central jet is more significant in the multineedle electrospinning process. As discussed above, for a given

Table 3. The measurement results of l_0, α_0, l_1, α_1, β in the multineedle electrospinning process

Applied Voltage (kV)	l_0 (cm)	α_0 (deg)	l_1 (cm)	α_1 (deg)	β (deg)
15	-	-	3.00	37.42	24.47
20	2.20	11.54	4.78	56.64	33.11
25	3.92	39.10	5.55	60.51	37.29

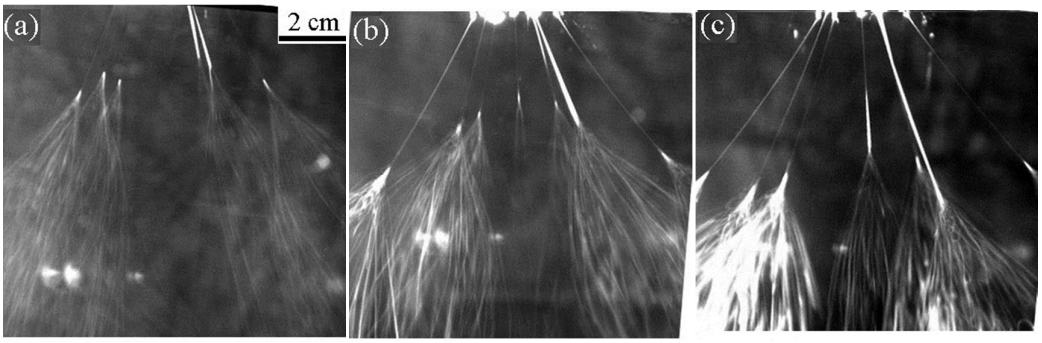

Fig. 11 The jet behaviors in the multineedle electrospinning process with various applied voltage: (a) 15 kV; (b) 20 kV; and (c) 25 kV.

configuration of the multijet electrospinning system, jet deviation depends on the balance of the Coulomb force and electric field force applied on the jet. A larger Coulomb force causes larger jet repulsion, while a larger electric field force results in a smaller jet offset. In multineedle electrospinning, the effect of Coulomb force overwhelms that of the electric field force. The Coulomb force and electric field force both increase with increasing electric field strength. From the electric field simulation results (shown in Figures 2 and 3), for the multineedle configuration, the electric field concentrates at the needle area. The large Coulomb force applied on the jet section near the spinneret results in significant jet repulsion, and therefore creates a large jet deviation angle. The electric field strength declines rapidly from the needle along the spinning direction. When reaching the whipping area, which is 30-60 mm away from the spinneret, the electric field strength created by the multineedle configuration is smaller than that for the multihole configuration. From Figure 8 and the related analysis, a small component of the electric field force along the *z*-axis can result in a larger envelop cone.

Conclusion

In this work, a comprehensive study was carried out to explore the effect of the electric field distribution on the jet motion and jet deviation in multijet electrospinning. For the jet motion, the results indicate that in multijet electrospinning, the central jet motion is depressed by the side jets surrounding it, and the stronger electric field leads to a longer straight jet length and a smaller envelope cone. Compared with the multihole configuration, the multineedle configuration creates much larger envelop cones and outer jet deviation angles.

The jet deviation occurs in multijet electrospinning is attributed to three factors: (1) the Coulomb force generated by the surface charge on the jet; (2) the diverging shape of the electric field lines; and (3) the electric field force applied on the jet. The surface charge and the electric field force depend on the electric field strength, while the electric field lines are determined by the configuration of the electrospinning system. It can be concluded that if the shape and strength of the electric field are well designed, jet behavior can be controlled in the multijet electrospinning process.

Acknowledgments

This work was financially supported by the National Natural Science Foundation of China (11272088), the Fundamental Research Funds for the Central Universities, and the Key grant Project of Chinese Ministry of Education (113027A).

References

1 Y. Yang, Z. Jia, L. Hou, J. Liu, L. Wang, Z. Guan, *IEEE Trans. Dielect. Electr. Insul.,* 2010, **17**, 1592-1601.
2 S. A. Theron, A. L. Yarin, E. Zussman, E. Kroll, *Polymer,* 2005, **46**, 2889-2899.
3 J. S. Varabhas, G. G. Chase, D. H. Reneker, *Polymer,* 2008, **49**, 4226-4229.
4 O.O. Dosunmu, G.G. Chase, W. Kataphinan, D.H. Reneker, *Nanotechnology,* 2006, **17**, 1123-1127.
5 F. Zhou, R. H. Gong, I. Porat, *Polym. Int.,* 2009, **58**, 331-342.
6 N. M. Thoppey, J. R. Bochinski, L. I. Clarke, R. E. Gorga, *Polymer,* 2010, **51**, 4928-4936.
7 K. M. Forward, G. C. Rutledge, *Chem. Eng. J.,* 2012, **183**, 492-503.
8 G. Jiang, S. Zhang, X. Qin, *Mater. Letters,* 2013, **106**, 56-58.
9 G. H. Kim, Y. S. Cho, W. D. Kim, *Eur. Polym. J.,* 2006, **42**, 2031-2038.
10 Y. Yang, Z. Jia, J. Liu, Q. Li, L. Hou, L. Wang, Z. Guan, *J. Appl. Phys.,* 2008, **103**, 104307.
11 S. Xie, Y. Zeng, *Ind. Eng. Chem. Res.,* 2012, **51**, 5336-5345.
12 J. M. Deitzel, J. D. Kleinmeyer, J. K. Hirvonen, N. C. Beck Tan, *Polymer,* 2001, **42**, 8163-8170.
13 A. Kumar, M. Wei, C. Barry, J. Chen, J. Mead, *Macromal. Mater. Eng.,* 2010, **295**, 701-708.
14 M. V. Kakade, S. Givens, K. Gardner, K. H. Lee, D. B. Chase and J. F. Rabolt, *J. Am. Chem. Soc.*, 2007, **129**, 2777-2782.
15 A. D. Winter, E. Larios, F. M. Alamgir, C. Jaye, D. Fischer and E. M. Campo, *Langmuir*, 2013, **29**, 15822-15830.
16 Y. Zheng, S. Xie, Y. Zeng, *J. Mater. Sci.,* 2013, **48**, 6647-6655.
17 Y. Zheng, X. Liu, Y. Zeng, *J. Appl. Polym. Sci.,* 2013, **130**, 3221-3228.
18 C. J. Angammana, S. H. Jayaram, *IEEE T. Ind. Appl.,* 2011, **47**, 1028-1035.
19 Y. M. Shin, M. M. Hohman, M. P. Brenner, G. C. *Polymer,* 2001, **42**, 9955-9967.
20 J. S. Lee, K. H. Choi, H. D. Ghim, S. S. Kim, D. H. Chun, H. Y. Kim, W. S. Lyoo, *J. Appl. Polym. Sci.,* 2004, **93**, 1638-1646.
21 D. H. Reneker, A. L. Yarin, H. Fong, S. Koombhongse, *J. Appl. Phys.,* 2008, **87**, 4531-4547.
22 Y. Zheng, Y. Zeng, *J. Mater. Sci.,* 2014, **49**, 1964-1972.

